Arch. Metall. Mater. **70** (2025), 3, 1383-1390

DOI: https://doi.org/10.24425/amm.2025.154491

I. CHADLI[1], A. CHADLI[2*] A. CHERIET[3], B. LAGOUN[4]

NEW INSIGHT INTO MECHANICAL STABILITY, ELECTRONIC AND ELASTIC PROPERTIES OF PARAELECTRIC *h*-$YMnO_3$ FROM FIRST-PRINCIPLES CALCULATIONS

In this work, we represent for the first time a study on h-$YMnO_3$ oxide in the para-electric phase using ab initio calculations, including equation of state, mechanical stability, electronic, magnetic and elastic properties. This theoretical study has been conducted using the full potential-linearized augmented plane wave method (FP-LAPW) within the framework of density functional theory (DFT). We also used the Tran-Blaha modified Becke-Johnson (TB-mBJ) for band structure calculations, as implemented in the wien2k code. Our calculations including internal atomic relaxations are in very good agreement with the available experimental data. Spin-polarized electronic band structure exhibits semiconductor behavior with a low band gap observed equal to 0.4 eV. The calculated elastic constants C_{ij} confirm the mechanical stability of our oxide. The estimated anisotropy factors show that *h*-$YMnO_3$ has a strong anisotropic character. To our knowledge, this is the first theoretical study on *h*-$YMnO_3$ oxide in paraelectric phase, which still awaits experimental confirmations.

Keywords: TB-mBJ; Multiferroics; paraelectric $YMnO_3$; Magnetic moment; Elastic constants

1. Introduction

Yttrium manganite $YMnO_3$, an insulator with low band gap which belongs to the hexagonal rare earth manganite ($RMnO_3$) (R = Ho – Lu, Y or Sc) [1,2]. It is the most attracted and the most intensively studied one because of its interested behaviours specially the multiferroic, in which ferroelectric and magnetic ordering occur simultaneously. Furthermore, this material demonstrates a frustrated magnetic ordering of Mn moments in conjunction with a layered crystal structure. In addition, this compound exhibits notable characteristics that are due to their compatibility with thin film growth techniques. An external electric field can modulate the ferroelectric component due to its perpendicular orientation to the ab-planes [3]. The *h*-$YMnO_3$ compound is used in several technological applications such as ferroelectric random-access memories FeRAM [4] and in metal-ferroelectric-insulator-semi-conductor layered structures MFIS for developing the field effect transistors [5].

Moreover, *h*-$YMnO_3$ is a type 1 multiferroic with a ferroelectric phase transition above 900 K (1000 K) and antiferromagnetic ordering at a much lower temperature of $T_N = 72$ K [5]. As mentioned in the work of Fujimura et al., at room temperature, the *h*-$YMnO_3$ is ferroelectric compound [6]. Whereas, Lukaszewicz et al., mentioned in their work that at the Curie temperature T_C =1273 K, the *h*-$YMnO_3$ undergoes a ferroelectric phase transition from a ferroelectric state with a non-centrosymmetric space group ($P6_3/cm$) to a paraelectric state with a centrosymmetric space group ($P6_3/mmc$). During this transition, the lattice constant c decreases as the temperature increases [7]. In addition, it was found without any doubt, the existence of a phase transition at 1000°C leading to the appearance of crystal structure with small hexagonal cell, which can be considered as a prototypical structure in relation to the ferroelectric structure of *h*-$YMnO_3$ at room temperature [7].

The crystal data of *h*-$YMnO_3$ above 1000°C shows that it has two formulas per unit cell, and the lattice constants have been estimated roughly as a = 3.61 Å and c = 11.39 Å [7]. Unfortunately, there is just one experimental study proposed by Lukaszewicz et al. (1974) about phase transition of *h*-$YMnO_3$ [7]. Elsewhere, very few theoretical studies are available in literature, except one established by Medvedeva et al. (2000) which focused the effect of Coulomb correlation and magnetic ordering on the electronic structure of two hexagonal phases of ferroelectromagnetic *h*-$YMnO_3$ [8]. Other theoretical study realized

[1] UNIVERSITY OF MOHAMED KHIDER, MATTER SCIENCES DEPARTMENT, 07000, BISKRA, ALGERIA
[2] UNIVERSITY OF MOHAMED KHIDER, LARHYSS LABORATORY, 07000, BISKRA, ALGERIA
[3] UNIVERSITY OF AMAR TELIDJI, LPCM LABORATORY, 03000 LAGHOUAT, ALGERIA
[4] UNIVERSITY OF AMAR TELIDJI, LPM LABORATORY, 03000 LAGHOUAT, ALGERIA

* Corresponding author: hakim.chadli@univ-biskra.dz

by Filippetti et al. (2001) about the structural, electronic and magnetic interplay in ferroelectromagnetic yttrium manganite (cubic and hexagonal in both AFM and NFM configurations) [9]. Hence, the ferroelectric structure has been the subject of our previous work [10,11] aiming several properties and behaviours of *h*-$YMnO_3$ at low temperature. Therefore, we propose in this paper a broad *ab initio* study of paraelectric *h*-$YMnO_3$. Since the study of various properties of solid or molecular devices using *ab initio* calculations has been the subject of many studies in recent years [12-17], we target the most fundamental physical properties such as mechanical stability, electronic, magnetic and elastic properties using density functional theory (DFT) and full-potential LAPW method. Furthermore, numerical estimates of the mechanical parameters such as Bulk modulus (B), shear modulus (G), Young's modulus (Y), compressibility (β), Poisson's ratio (ν) and Lamé coefficients (μ, λ) of the paraelectric oxide *h*-$YMnO_3$ in the Voigt-Reuss-Hill approximations were obtained and analyzed for the first time.

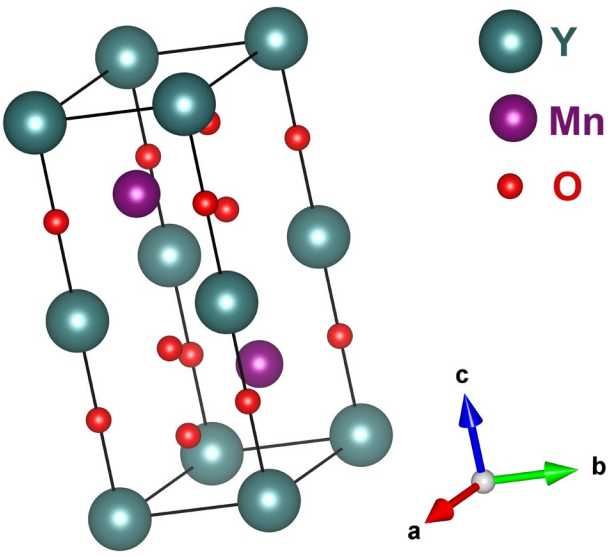

Fig. 1. Representation of para-electric h-$YMnO_3$ crystal structure; using Vesta software [20]

2. Computational details

Based on previous successes in describing the ground state properties of different materials using *ab initio* calculations [18-19]. The computational analyses were conducted using the Kohn-Sham Density Functional Theory (DFT) framework [21,22] and the full-potential linearized augmented plane-wave method (FP-LAPW) [23] as implemented in the Vienna package wien2k [24]. Initially, the electronic exchange-correlation interactions were treated using Generalized Gradient Approximation (GGA) with the Perdew-Burke-Ernzerhof (PBE96) functional [25]. We have also utilized the Tran-Blaha modified Becke-Johnson (TB-mBJ) potential [26] to improve the precision of electronic structure calculations. The plane-wave cut-off parameter $R_{MT} \times K_{max}$ was set to be 7, where R_{MT} represents the smallest muffin-tin sphere radius and K_{max} is the maximum value of the plane-wave vector. The atomic wave functions within the muffin-tin spheres were expanded up to an angular momentum quantum number of $l_{max} = 10$, and the number of *k*-points used in the irreducible part of the Brillouin zone (BZ) is 400 *k*-points by means of Monkhorst-Pack grid [27]. Moreover, the muffin-tin radii R_{MT} were set to: 2.1, 1.75, and 1.60 Bohr for the Y, Mn and O atoms, respectively, and the configuration of valence electrons was $5s^2 4d^1$ for Y, $4s^2 3d^5$ for Mn and $2s^2\ 2p^4$ for O. In order to ensure very high quality of our results, the calculations were assured a high-level convergence of the total energy difference within 10^{-6} Ry and maximum Hellmann Feynman force within 1.0 Ry/Bohr. We have chosen these computational methods and parameters to ensure and guarantee robust and reliable results, consistent with established best practices in computational materials science.

3. Results and discussion

3.1. Structural study

The ideal structure of para-electric *h*-$YMnO_3$ crystal has been fully optimized in different spin configurations such as ferromagnetic (FM), antiferromagnetic (AFM) and non-ferromagnetic (NFM) by minimizing the total energy vs volume using the only available experimental data [7], taking into account the optimization of the c/a ratio. Then, we carried calculations for the relaxation of the structure by minimizing the Hellmann-Feynman forces and were reduced less than 1.0 m Ry/Bohr. The results of our calculations and experimental one of the lattice parameters and the bulk modulus B are listed in TABLE 1, where the experimental and calculated atomic positions are summarized in TABLE 2.

TABLE 1

Ground state optimized structural parameters including the lattice constant (a and c, in Å), volume (V, in Å^3), c/a ratio (without unity), the total energy and the total energy difference (AFM as reference) (E, and $\Delta E_{i/AFM}$, in Ry), Bulk modulus and its derivate (B, in GPa and B', without unity)

	Spin configuration	a	c	V	c/a	E	$\Delta E_{i/AFM}$	B	B'
This work	FM	3.602	11.364	127.687	3.155	–19081.627	0.004	176.22	4.73
	AFM	3.586	11.412	127.100	3.182	–19081.631	0.000	176.67	4.68
	NFM	3.571	11.378	125.655	3.186	–19080.547	1.0785	177.43	4.54
Other work [9]	NFM	3.518	11.29	120.00	3.209	—	—	—	—
Exp. [7]	—	3.61	11.39	128.54	3.155	—	—	—	—

According to the data summarized in TABLE 1, we can observe that all obtained values for the lattice constants (FM: a = 3.602 and c =11.364 Å, AFM: a = 3.586 and c = 11.412 Å and NFM: a = 3.571 and c =11.378 Å) are smaller compared to the experimental data (a = 3.61 and c = 11.39 Å). Whereas, the deviation in *a* parameters is about 0.008, 0.024 and 0.039 Å for FM, AFM and NFM respectively, and in c parameter is about 0.026, –0.022 and 0.012 Å for FM, AFM and NFM, respectively. The calculated c/a ratio for FM configuration is exactly equal to the experimental value of about 3.155 for, while for AFM and NFM configuration is about 3.182 and 3.186 respectively. Therefore, the unit equilibrium volume is underestimated by 0.66%, 1.12% and 2.24% for FM, AFM and NFM respectively. Furthermore, in terms of energy, our results show that the AFM and FM configurations are the most stable one with a slight preference for AFM ($\Delta E_{FM/AFM}$ = 0.04 Ry), while for the NFM configuration $\Delta E_{NFM/AFM}$ is about 1.078 Ry. The calculated atomic positions gathered in TABLE 2 are very similar to the available experimental one [7]. Fig. 2 shows the variations of total energy (E) versus primitive unit cell volume (V) in FM, AFM and AFM configuration adapted under the Murnaghan equation of state (Eq. (1)) [28]:

$$E(V) = E_0 + \left(\frac{BV}{B'} \left(\frac{1}{B'-1)} \left(\frac{V_0}{V} \right)^{B'} + 1 \right) - \frac{BV_0}{B'-1} \right) \qquad (1)$$

Where, E_0 represents energy at the lowest stable state and V_0 the equilibrium volume, *B* denotes the bulk modulus in GPa and *B′* represents the pressure derivative of the bulk modulus. The calculated values of the bulk modulus *B* tabulated in TABLE 1, is about 176.22, 176.67 and 177.43 GPa for FM, AFM and NFM respectively. We note that there is no data available of *B* for our oxide in the paraelectric phase; therefore, our results are predictions, and are compared with that of ferroelectric phase of about 169.9 and 171.3 GPa for FM and AFM configurations respectively [11] and that observed in $SrZrO_3$ perovskite of about 171 GPa reported in reference [29]. Based on these obtained results, which show that the AFM and FM configurations are the most stable and that the FM configuration unit cell parameters are most comparable one to the experimental data, we'll focus only on the FM configuration in what follows, to achieve the different properties and behaviours of *h*-$YMnO_3$ oxide at high temperature.

3.2. Electronic properties

a. Band structure

Fig. 3 shows the calculated band structure of paraelectric *h*-$YMnO_3$ along the high-symmetry directions in the Brillouin zone (Γ-M-K-Γ-A-L-H-A/L-M/K-H) [30] for the FM configuration using the approximation GGA+mBJ, after a good relaxation

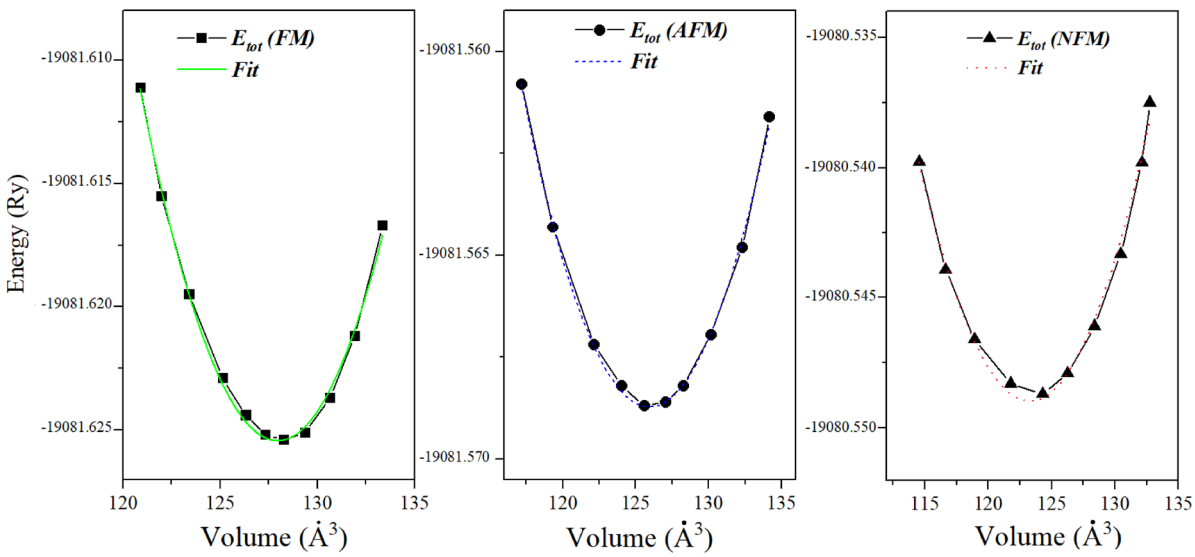

Fig. 2. Optimized crystallographic structures with energy-volume (E–V) plots for h-$YMnO_3$ in FM, AFM and NFM configuration

TABLE 2

Experimental atomic positions and calculated one

Atoms	This work									Exp. [7]		
	AFM			FM			NFM					
	x	y	x	x	y	x	x	y	x	x	y	z
Y	0	0	0	0	0	0	0	0	0	0	0	0
Mn	1/3	2/3	¼	1/3	2/3	¼	1/3	2/3	¼	1/3	2/3	1/4
O(1)	0	0	¼	0	0	¼	0	0	¼	0	0	1/4
O(2)	1/3	2/3	0.836	1/3	2/3	0.842	1/3	2/3	0.836	1/3	2/3	0.84

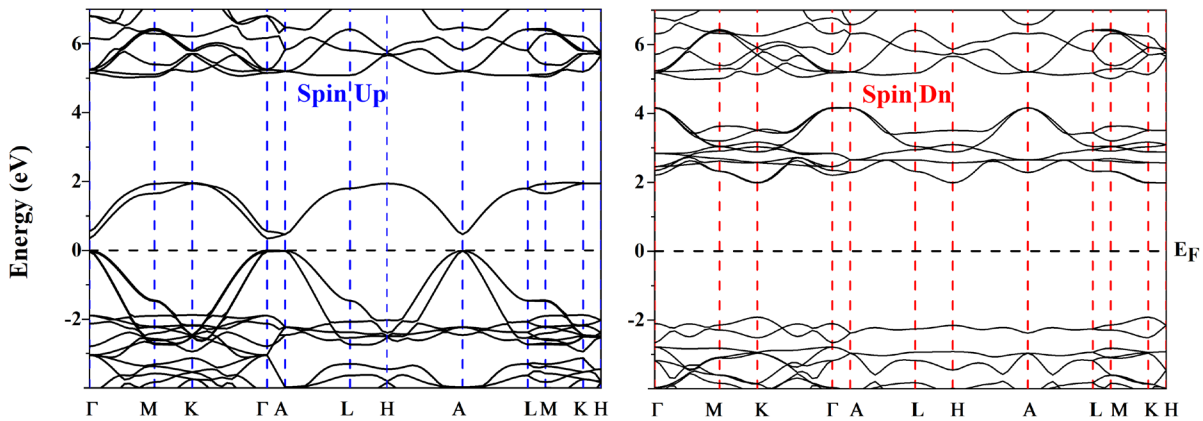

Fig. 3. Band structure of para-electric h-$YMnO_3$ using GGA+mBJ approximation

of the optimized structure. First, using GGA approximation, no band gap was observed for the spin up and spin down, which reflects a metallic behaviour of our material; whereas the implementation of the mBJ potential points out a direct band gap located at Γ point was observed of about 0.4 and 3.8 eV for the spin up and spin down, respectively. This observed low gap can be taken as an indication of a pseudo-Jahn-Teller effect, arising in the case where the d levels have an energy separation. It should be noted that there is no available experimental band gap to compare with the calculated one, hence, our results are compared those mentioned by J.E. Medvedeva et al., about 0.01 eV for the FM configuration [8]. While Filippetti et al., mentioned in their work that the paraelectric antiferromagnetic *h*-$YMnO_3$ has a metallic behaviour with band gap equal to zero [9].

b. Density of states and electronic density

The total and partial density of state (DOS and PDOS) of paraelectric *h*-$YMnO_3$ calculated using GGA+mBJ approximation are illustrated in Fig. 4. It can be seen that the magnetic character of our material is clearly visible in the total DOS. Indeed, the states of spin up and spin down are not symmetrical, which reveals a non-zero magnetic moment for paraelectric *h*-$YMnO_3$ oxide as reported in other work [8,31]. Other main observe is the presence of the gap close to the Fermi level E_F (taken as energy reference) of about 0.4 eV which confirms the semi-conductor character of our material. This weak band can be due to muffin-tin approximation [32]. In addition, the analysis details point out that no difference is observed in the Y PDOS shape for major spin and minor spin, which indicates that the magnetic moment of yttrium atome is negligible. From the density of states, the valence band (VB) extends from –7 eV to 0 eV is dominated by 3d (Mn) states with a good contribution of 2p (O) states and small of the 4d (Y). Such interaction between cation and anion orbitals results in covalent bonding in Mn-O and Y-O with ionic character. A similar interaction between 2p (O) and 3d (Mn) states is less observed in the conduction band (CB). Where, the presence of 4d (Y) states in the conduction band with wide peaks between 5 and 6.5 eV, indicating a charge transfer from the 4d (Y) states to the states of anionic atoms which is the 2p (O), which reflects an ionic character of the Y-O bonding.

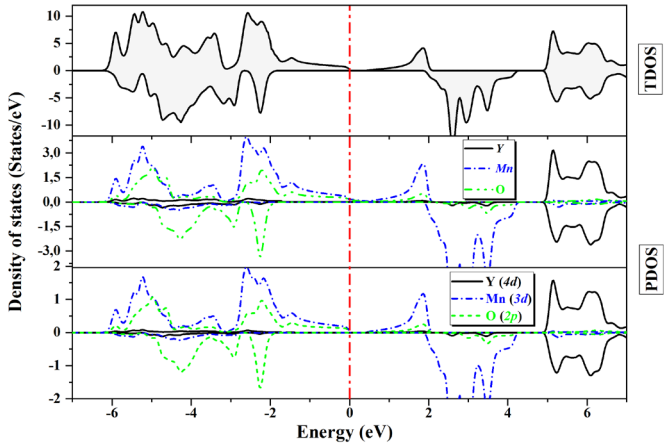

Fig. 4. TDOS and PDOS of para-electric h-$YMnO_3$

This result can be confirmed by the electronic density, which can be further analysed by examining the charge distribution between different atoms. The existence of a significant hybridization between 3d (Mn) and 2p (O) states in *h*-$YMnO_3$, means that the bonding in our system cannot be purely ionic but must exhibit a large covalent part.

To have a clearer idea of the nature of the chemical bond between the different atoms of *h*-$YMnO_3$ in the paraelectric phase, we have represented the distribution of charge density in a plane contains yttrium, magnesium and oxygen atoms in Fig. 5. using XCrySDen software [33]. Fig. 5. shows a sharing of charge between Mn and O due to 3d (Mn) and 2p (O) hybridization. Where the distribution of charge around Y site indicates that the bonding between Y and MnO_3 is mainly ionic.

3.3. Magnetic properties

The magnetic moment in a material is due to the spin configuration of an electron, if the spin up state has no (or negligible) band gap in a material and the spin down state has a remarkable

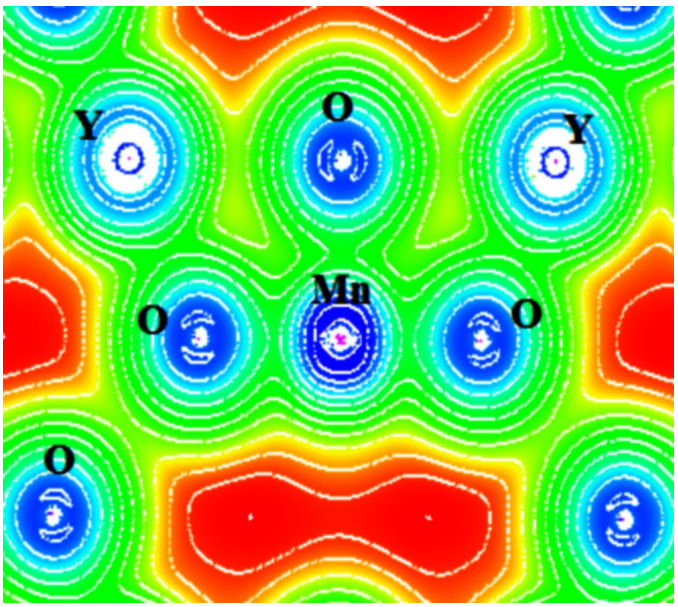

Fig. 5. The valence charge density contour for paraelectric h-$YMnO_3$

band gap, then the material is a half-metallic ferromagnetic and exhibits full spin polarization at the Fermi level. This phenomenon is well known as spin polarization, making the spintronics a growing field of research with many applications. Therefore, various high-quality magneto-electronic and processing devices have been developed using the concept of spintronics.

Using the optimized lattice parameters values leads us to determine the magnetic properties. It is well known that the total magnetic moment in compounds is the sum of the magnetic moments of the different atoms [34,35]. Generally, the Mn layers in $RMnO_3$ compounds play an important role in evaluating of their magnetic moment [8,31]. The total magnetic moment of paraelectric *h*-$YMnO_3$ oxide is about 8.00 and 3.63 μB per unit cell and formula respectively using both approximations GGA and GGA+mBJ. Whereas, the magnetic moment of Mn atom is about 3.25 and 3.26 μB using GGA and GGA+mBJ, respectively, in good agreement with available theoretical (3.8 and 3.5 μB [8,29,31]) and with the experimental one (2.9 μB [36]). These values of Mn magnetic moment, which is slightly smaller than the total magnetic moment, are mainly due to the localization of the spin polarized charge around the manganese atom. We note here that the contribution of Y and O atoms is not meaningful, however, on-negligible magnetic moments are observed for O atoms about -0.04 μB, while the magnetic moments for Y atoms is negligible about 0.008 μB. Another interesting property is the magneto-elasticity, which aims to study the effect of pressure on the total magnetic moment. For this reason, we performed FP-LAPW calculations on the *h*-$YMnO_3$ oxide on different volumes (pressures), then, we calculated the corresponding magnetic moment using the GGA approximation. The variation of the total magnetic moment per unit cell as a function of pressure shows a slight decrease of the total magnetic moment when the pressure increases from 0 to ~9.5 GPa, which reflects and predict the presence of a magnetic reactivity of the paraelectric *h*-$YMnO_3$ relative *vs*. an applied pressure.

3.4. Mechanical properties

a. Elastic constants and polycrystalline moduli

Density functional theory calculations (DFT) have been successfully utilized to compute phase stability as well as elastic properties of several compounds [37-39]. Therefore, we calculated the five elastic constants (C_{11}, C_{12}, C_{13}, C_{33} and C_{44}) for the hexagonal paraelectric *h*-$YMnO_3$ via stress-strain relations with ±d % (d = 0.1, 0.2, and 0.3) strains applied in the uniaxial regime, separately for each C_{ij}. The elastic constants C_{ij} calculated using Wien2k and ABINIT packages [24,40] are presented in TABLE 3. For stable hexagonal structure, the independent elastic constants should satisfy the well-known Born stability criteria [41]. The calculated elastic constants presented in TABLE 3 are positive and they clearly satisfy the Born stability criteria, suggesting that the paraelectric *h*-$YMnO_3$ (FM) structure is mechanically stable.

TABLE 3

Elastic constants (GPa) of para-electric *h*-$YMnO_3$ in FM configuration

Elastic Constants (GPa)	C_{11}	C_{12}	C_{13}	C_{33}	C_{44}	C_{66}
This work (Wien2K)	280	187.2	97.7	283.5	73	46.4
This work (ABINIT)	291	113	113	312	101	89
Exp. (at 4 K) [42]	185	66.2	—	298	98.6	59.4

Then, we have derivate other elastic quantities which are related to the elastic constants, such as Bulk modulus B, shear modulus G, Young's modulus Y, Poisson's ratio υ, and the Lamé constants (λ and μ) following the equations considered within the Voigt-Reuss-Hill methods and relations summarised in ref [10]. These quantities calculated using ABINIT and Wien2k packages are presented in TABLE 4.

It is well known that the both shear and bulk moduli measure of the hardness of a solid. A material is brittle (ductile) if the B/G ratio is less (greater) than 1.75. In fact, the value of B/G is about 2.6 and 2.3 (using wien2K and ABINIT respectively), consequently, our material in the paraelectric phase should behave in a ductile behavior, but less than the one observed for the ferroelectric phase with B/G about 1.91 [10]. The calculated Young's modulus (Y) which is also a parameter that measures the stiffness of a material is approximately 178 GPa (also 199 GPa using abinit) confirming that our oxide in PE phase retains its noted rigidity in FE phase. In addition, Lamé parameters are the Lamé constant (closely related to incompressibility) (λ) and shear rigidity (μ) [43], in which are derived from the elasticity moduli and Poisson's ratio. Physically, the shear modulus (G) and shear rigidity (μ) are equal and give information about shear stiffness of materials while the Lamé constant (λ) is related to the compressibility of the mater [44]. We note here, that no experimental or other theoretical data for the different modulus of paraelectric *h*-$YMnO_3$ are available; therefore, we consider the present results as a prediction study.

TABLE 4

Calculated values of some elastic parameters for para-electric h-$YmnO_3$ oxide as obtained in VRH approximation: bulk modulus (B), shear modulus (G), Young's modulus (Y) and Lamé constants (λ and u) in GPa, compressibility (β) in GPa^{-1} and Poisson's ratio (ν) without unity

Modulus	This work	
	Wien2K	ABINIT
B_V	174.7	178.7
B_R	174.5	176.2
B_{VRH}	174.6	177.5
β	0.006	0.005
G_V	95.2	69.2
G_R	94.9	62.53
G_{VRH}	95	65.86
Y	241.3	175.8
ν	0.27	0.33
λ	111.23	133
μ	95	65.7

As we observed in the electronic properties of the bonding nature, another factor that confirms the ionic behaviour of our material is the Poisson's ratio (***ν***); its value indicates the degree of directionality of the covalent bonds. A small value ($\nu = 0.1$) for covalent materials, whereas for the ionic materials a typical value of ***ν*** is 0.25 [45]. In our case, the values of ***ν*** for paraelectric h-$YMnO_3$ oxide is at about 0.33 (also 0.31 using abinit), therefore, the ionic contribution to the interatomic bonding is dominant. It should be noted that the same behavior was observed for the ferroelectric phase [10].

b. Anisotropy of elastic factors

Most crystals exhibit elastic anisotropies of varying degree and there are several methodologies can be used to indicate the elastic anisotropy in hexagonal crystals. The different factors of elastic anisotropy calculated in the present work using two packages Wien2k and ABINIT, are summarised in TABLE 5. First, we can easily see that the elastic constant C_{33} value is greater than that of C_{11}. Thus, we can consider that the *a*-axis is more compressible than the *c*-axis in these compounds, and that there are strong chemical bonds along the [001] direction for our oxide.

The Zener anisotropy factor A is an indicator of the degree of anisotropy in the solid structure compared to the isotropic material. For the hexagonal structure there are two Zener anisotropy factors; firstly, A_1 which is the shear anisotropy factor for the {1 0 0} shear planes between the ⟨011⟩ and ⟨010⟩ directions. Secondly, A_2 which is the shear factor in the {0 0 1} shear planes between ⟨110⟩ and ⟨010⟩ directions [46]. A crystal with A_1 and A_2 values equal to 1 is isotropic, otherwise, it is anisotropic. Therefore, it is clear from the TABLE 5 that both factors A_1 and A_2 are less than 1, which confirms that the h-$YMnO_3$ crystals exhibit a good anisotropy in different directions, with an anisotropy in the (100) plane bigger than that in the plane (001).

The universal anisotropy index A^U, and the percentages anisotropy in compression A_{comp} and in shear A_{shear} which can be used to quantify the single crystal elastic anisotropy were calculated using relations mentioned in ref [10]. For isotropic structures, the Voigt and Reuss approximations should give the same values for B and G, respectively. Therefore all of the indices of A^U, A_{comp} and A_{shear} are zero. Deviations from zero indicate the degree of anisotropy of the material. Since all numerical values of A^U , A_{comp} and A_{shear} listed in TABLE 5 are bigger than zero, therefore our crystal h-$YMnO_3$ should have anisotropic behaviour.

In addition, we can by solving the Christoffel equation, getting out the anisotropy of the compression wave (Δ_P), the anisotropies of the shear wave polarized perpendicular to the basal plane (Δ_{S1}) and that polarized in the basal plane (Δ_{S2}). For Δ_{S2} and Δ_P waves, the extreme occurs along the c axis, for Δ_{S1} it is at an angle of 45° from the c axis in the a-c plane. A crystal with: $\Delta_P = \Delta_{S1} = \Delta_{S2} = 1$, is isotropic, while all values other than unity represent the degrees of anisotropy [47]. Our obtained values of Δ_P, Δ_{S1} and Δ_{S2} are different from one (1.19, 1.26 and 1.49), which confirms the anisotropic character of h-$YMnO_3$ oxide in the paraelectric phase.

4. Conclusion

In this work, we have performed *ab initio* analysis using DFT-FP-LAPW method, GGA and GGA+mBJ approximations on the structural, electronic, magnetic and elastic properties of para-electric h-$YMnO_3$ in ferromagnetic configuration. A summary of the main findings follows:

- The calculated lattice constants are in excellent agreement with the available experimental data.
- The calculated band structure shows a metallic and half-metallic character using GGA and GGA+mBJ approximations respectively, where using GGA+mBJ a direct band gap equal to 0.4 eV was observed, which makes h-$YMnO_3$ oxide a candidate for spintronics applications. Whereas, the calculated DOS confirms the ferromagnetic character and indicates a covalent-ionic character in the bonding Mn-O and Y-O, respectively.

TABLE 5

The shear anisotropy factors A_1 and A_2, universal anisotropy index A^U, percentages of anisotropy in compression A_{comp} and in shear A_{shear}, the compression wave Δ_P, and shear wave anisotropy Δ_{S1} and Δ_{S2} of para-electric h-$YMnO_3$

Anisotropic factors	A_1	A_2	A^U	A_{comp}	A_{shear}	Δ_p	Δ_{S1}	Δ_{S2}
This work (Wien2K)	0.0017	0.0068	0.54	0.64	4.30	1.01	1.26	1.49
This work (Abinit)	0.0031	0.0065	0.028	0.62	0.15	1.19	1.01	1.04

- The calculated magnetic moment of our oxide, agree well with the experimental one for all adopted approximations. The magnetism in the *h*-$YMnO_3$ due mainly to the Mn element because it has the highest partial magnetic moment of about 3.26 μB.
- The study of the effect of pressure on the total magnetic moment shows the presence of a magnetic reactivity of *h*-$YMnO_3$ relative to an applied pressure.
- The calculated elastic constants obey the mechanical stability conditions, confirming the mechanical stability of our oxide and the ideal polycrystalline aggregates bulk modulus, shear modulus, Young's modulus and all the calculated anisotropy factors confirm the order anisotropic of our material.

Acknowledgements

The authors wish to thank the Laboratory of Physico-chemistry of materials, Laghouat University, Algeria, for providing adequate working conditions to accomplish this work.

REFERENCES

[1] T. Tajiri, H. Deguchi, M. Mito, A. Kohno, The Journal of Physical Chemistry C **125** (26), 14474-14485 (2021). DOI: https://doi.org/10.1021/acs.jpcc.1c03497

[2] S. Xing, S. Song, J. Xiang, Russian Journal of Physical Chemistry **95**, 1033-1042 (2021. DOI: https://doi.org/10.1134/S0036024421050241

[3] N. Fujimura, T. Ishida, T. Yoshimura, T. Ito, Appl. Phys. Lett. **69** 1011 (1996). DOI: https://doi.org/10.1063/1.117969

[4] A.G. Kochur, A.T. Kozakov, K.A. Googlevb, A.V. Nikolskii, Journal of Electron Spectroscopy and Related Phenomena **195**, 1-7 (2014). DOI: https://doi.org/10.1016/j.elspec.2014.04.007

[5] T. Choi, J. Lee, Appl. Phys. Lett. **84**, 5043-5045 (2004). DOI: https://doi.org/10.1063/1.1763642

[6] N. Fujimura, T. Ishida, T. Yoshimura, T. Ito, Appl. Phys. Lett. **69**, 1011-1013 (1996). DOI: https://doi.org/10.1063/1.117969

[7] K. Lukaszewicz, J. Karut-Kalicinska, Ferroelectrics **7**, 81-82 (1974). DOI: https://doi.org/10.1080/00150197408237954

[8] J.E. Medvedeva, V.I. Anisimov, M.A. Korotin, O.N. Mryasov, A.J. Freeman, J. Phys.: Condens. Matter **12**, 4947-4958 (2000). DOI: https://doi.org/10.1088/0953-8984/12/23/304

[9] A. Filippetti, N.A. Hill, Journal of Magnetism and Magnetic Materials **236** (1-2), 176-189 (2001). DOI: https://doi.org/10.1016/S0304-8853(01)00445-0

[10] A. Chadli, M. Halit, B. Lagoun, F. Mohamedi, S. Maabed, A. Cheriet, E. Hlil, Solid State Phenom. **297**, 120-130 (2019). DOI: https://doi.org/10.4028/www.scientific.net/SSP.297.120

[11] A. Chadli, B. Lagoun, L. Aissani, S. Khenchoul, I. Chadli, R. Makhloufi, E.K. Hlil, Journal of Electronic Materials **50** (2), 657-663 (2021). DOI: https://doi.org/10.1007/s11664-020-08592-y

[12] A. Azouaoui, A. Harbi, M. Moutaabbid, M. Idiri, A. Eddiai, N. Benzakour, A. Rezzouk, Indian Journal of Physics **97** (6), 1727-1737 (2023). DOI: https://doi.org/10.1007/s12648-022-02522-w

[13] I.A. Elkoua, R. Masrour, Optical and Quantum Electronics **54** (10), 667 (2022). DOI: https://doi.org/10.1007/s11082-022-03999-9

[14] M.Y, Raïâ, R. Masrour, M. Hamedoun, J. Kharbach, A. Rezzouk, A. Hourmatallah, N. Benzakour K. Bouslykhane, Nanoscale and Microscale Thermophysical Engineering **27** (1), 1-24 (2023). DOI: https://doi.org/10.1080/15567265.2023.2167532

[15] A.F. Kisomi, S.J. Mousavi, B. Nedaee-Shakarab, Archives of Metallurgy and Materials **68** (3), 875-880 (2023). DOI: https://doi.org/10.24425/amm.2023.145450

[16] H. Rezazadeh, M. Hantehzadeh, A. Boochani, Archives of Metallurgy and Materials **67** (1), 155-166 (2022). DOI: https://doi.org/10.24425/amm.2022.137484

[17] A. Bagheri, A. Boochani, S.R. Masharian, F.H. Jafarpour, Archives of Metallurgy and Materials **68** (1), 331-338 (2023). DOI: https://doi.org/10.24425/amm.2023.141509

[18] M.Y, Raïâ, R. Masrour, M. Hamedoun, J. Kharbach, A. Rezzouk, A. Hourmatallah, N. Benzakour K. Bouslykhane, Optical and Quantum Electronics **55**, 512 (2023). DOI: https://doi.org/10.1007/s11082-023-04793-x

[19] M.Y, Raïâ, R. Masrour, M. Hamedoun, J. Kharbach, A. Rezzouk, A. Hourmatallah, N. Benzakour K. Bouslykhane, Journal of Materials Science: Materials in Electronics **33**, 20229-20256 (2022). DOI: https://doi.org/10.1007/s10854-022-08841-2

[20] J.K. Momma, F. Izumi, J. Appl. Crystallogr. **44**, 1272 (2011). DOI: https://doi.org/10.1107/S0021889811038970

[21] P. Hohenberg, W. Kohn, Phys. Rev. **136**, B864-B870 (1964). DOI: https://doi.org/10.1103/PhysRev.136.B864

[22] W. Kohn, L.J. Sham, Phys. Rev. **140**, A1133-A1138 (1965). DOI: https://doi.org/10.1103/PhysRev.140.A1133

[23] O.K. Andersen, Phys. Rev. B. Condens Matter, **12**, 3060-3083 (1975. DOI: https://doi.org/10.1103/PhysRevB.12.3060

[24] K. Schwarz, P. Blaha, G.K. Madsen, Comp. Phys. Comm. **147**, 71-76 (2002). DOI: https://doi.org/10.1016/S0010-4655(02)00206-0

[25] J.P. Perdew, S. Burke, M. Ernzerhaf, Phys. Rev. Lett. **77**, 3865-3868 (1996). DOI: https://doi.org/10.1103/PhysRevLett.77.3865

[26] D. Koller, F. Tran, P. Blaha, Physical Review **85**, 155109 (2012). DOI: https://doi.org/10.1103/PhysRevB.85.155109

[27] H.J. Monkhorst, J.D. Pack, Physical Review B **13** (12), 5188 (1976). DOI: https://doi.org/10.1103/PhysRevB.13.5188

[28] F.D. Murnaghan, Proceedings of National Academy of Sciences **30** (9), 244-247 (1944). DOI: https://doi.org/10.1073/pnas.30.9.244

[29] E. Mete, R. Shaltaf, S. Ellialtıoğlu, Physical Review B **68** (3), 035119 (2003). DOI: https://doi.org/10.1103/PhysRevB.68.035119

[30] W. Setyawan, S. Curtarolo, Comput. Mat. Sc. **49**, 299-312 (2010). DOI: https://doi.org/10.1016/j.commatsci.2010.05.010

[31] M. Qian, J. Dong, Q. Zheng, Physics Letters A **270**, 96-101 (2000). DOI: https://doi.org/10.1016/S0375-9601(00)00287-5

[32] F.M. Michel-Calendini, H. Chermette, J. Weber, Journal of Physics C: Solid State Physics **13** (8), 1427 (1980). DOI: https://doi.org/10.1088/0022-3719/13/8/013

[33] A. Kokalj, Journal of Molecular Graphics and Modelling **17** (3-4), 176-179 (1999). DOI: https://doi.org/10.1016/S1093-3263(99)00028-5

[34] M.Y. Raïâ, R. Masrour, M. Hamedoun, J. Kharbach, A. Rezzouk, A. Hourmatallah, N. Benzakour, K. Bouslykhane, Solid State Communications **355**, 114932 (2022). DOI: https://doi.org/10.1016/j.ssc.2022.114932

[35] M.Y. Raïâ, R. Masrour, M. Hamedoun, J. Kharbach, A. Rezzouk, A. Hourmatallah, N. Benzakour, K. Bouslykhane, Applied Physics A **129**, 493 (2023) DOI: https://doi.org/10.1007/s00339-023-06744-5

[36] T. Lancaster, S.J. Blundell, D. Andreica, M. Janoschek, B. Roessli, Physical review Letters **98** (19), 197203 (2007). DOI: https://doi.org/10.1103/PhysRevLett.98.197203

[37] S. A.Khandy, I. Islam, A.Laref, M. Gogolin, A. K. Hafiz, International Journal of Energy Research **44** (4), 2594-2603 (2020). DOI: https://doi.org/10.1002/er.4982

[38] M.Y. Raïâ, Masrour, R. Hamedoun, M.J. Kharbach, A. Rezzouk, A. Hourmatallah, N. Benzakour, K. Bouslykhane. J. Supercond. Nov. Magn. **36**, 349-365 (2023). DOI: https://doi.org/10.1007/s10948-022-06473-5

[39] O. Kabi, M.S. Abu-Jafar, M. Farout, A.A. Mousa, A. Bouhemadou, N. Erum, ACS Omega **9** (10), 11820-11828 (2024). DOI: https://doi.org/10.1021/acsomega.3c09292

[40] X. Gonze, J.-M. Beuken, R. Caracas, F. Detraux, Comput. Mat. Sci. **25**, 478 (2002). DOI: https://doi.org/10.1016/S0927-0256(02)00325-7

[41] J.F. Nye, Physical properties of crystals: their representation by tensors and matrices. Oxford University Press, UK, 1985.

[42] M. Poirier, F. Laliberté, Physical Review B **76**, 174426 (2007). DOI: https://doi.org/10.1103/PhysRevB.76.174426

[43] W. Baoli, Y. Xingyao, Z. Fanchang, Applied Geophysics **3** (3), 174-178 (2006). DOI: https://doi.org/10.1007/s11770-006-0026-z

[44] I.R. Shein, A.L. Ivanovski, Journal of Physics: Cond. Matt. **20** (41), 415218 (2008). DOI: https://doi.org/10.1088/0953-8984/20/41/415218

[45] V.V. Bannikov, I.R. Shein, A.L. Ivanovskii, Physica Status Solidi **1** (3), 89-91 (2007). DOI: https://doi.org/10.1002/pssr.200600116

[46] P.W.O. Nyawere, N.W. Makau, G.O. Amolo, Physica B. **434**, 122-128 (2014). DOI: https://doi.org/10.1016/j.physb.2013.10.051

[47] R. Li, Y. Duan, Philosophical Magazine **96** (35), 3654-3670 (2016). DOI: https://doi.org/10.1080/14786435.2016.1234081

Received 29 December 2024; Received in revised form 3 March 2025; Accepted 3 March 2025